Energy 315 (2025) 134428

Contents lists available at ScienceDirect

Energy

journal homepage: www.elsevier.com/locate/energy

Experimental investigation on an advanced thermosiphon-based heat exchanger for enhanced waste heat recovery in the steel industry

Hussam Jouhara [a,b,*], Bertrand Delpech [a], Sulaiman Almahmoud [a], Amisha Chauhan [a], Fouad Al-Mansour [c], Matevz Pusnik [c], Alojz Buhvald [d], Kristijan Plesnik [d]

[a] Heat Pipe and Thermal Management Research Group, Brunel University London, Uxbridge, UB8 3PH, UK
[b] Vytautas Magnus University, Studentu Str. 11, Kaunas Distr., LT-53362, Akademija, Lithuania
[c] Josef Stefan Institute, Energy Efficiency Centre, 1000, Ljubljana, Slovenia
[d] SIJ METAL RAVNE, Koroška cesta 14, 2390, Ravne na Koroškem, Slovenia

A B S T R A C T

Industry sector within the European Union (EU) accounts for approximately 25 % of final energy use, where the steel industry accounts for 10 % of the total energy consumption in the industry sector. The steel industry and similar process industries are facing significant challenges to reduce their greenhouse gas emissions due to recent climate change legislations. One method to achieve this, is via the implementation of waste heat recovery systems. The paper presented focuses on a steel plant located in Slovenia, where significant amounts of thermal energy are lost through exhaust gases from a natural gas furnace. The novel multi-sink gravity-assisted Heat Pipe Heat Exchanger (HPHE) aims to recover and reuse waste heat and generates two useful heat sinks. The novel HPHE consists of air and water heat sink sections with an average energy recovery efficiency of 47 %. The recovered energy from the air section provides preheated combustion air to the burners, whereas the recovered energy from the water section opens the possibility for district heating. The thermosyphons in the exhaust-air section were arranged in a counterflow arrangement with Dowtherm A and distilled water as the working fluid, whereas the exhaust-water sections were arranged in a crossflow, with distilled water as the working fluid. The novel HPHE features a bypass, allowing complete flexibility for the end user to deactivate the exhaust-water section. To ensure replicability of the HPHE, a theoretical model has been developed and validated through experimental results, the model exhibited a good agreement with the results within an error of 15 %. Both air and water sections recovered 1677 MWh and 753 MWh annually, operating at 8050 and 5750 h respectively. The implementation of the HPHE equates to an overall reduction in CO2 emissions of 334 tCO2 per annum. Moreover, the unit highlights a benchmark for the technology due to its readiness within industry due to a reported Return on Investment (ROI) of under 10 months.

Nomenclature

Symbols		Unit
A	Surface area	m^2
C	Heat capacity rate	$W.K^{-1}$
Cst	Cost	£.$year^{-1}$
C_P	Specific heat capacity	$J.kg^{-1}.K^{-1}$
C_r	Heat capacity ratio, $(C_r = C_{min}/C_{max})$	dimensionless
C_{sf}	Constant in *Rohsenow* correlation depending on the surface-fluid combination	dimensionless
D	Diameter	m
E	Energy	kWh
g	Gravitational acceleration	$m.s^{-2}$
h	Heat transfer coefficient	$W.m^{-2}.K^{-1}$
h_{fg}	Latent heat of vaporisation	$J.kg^{-1}$
k	Thermal conductivity of the heat pipe wall	$W.m^{-1}.K^{-1}$
L	Length	m
$\dot{m}$	Mass flow rate	$kg.s^{-1}$

(*continued on next column*)

(*continued*)

Symbols		Unit
n_{total}	Number of pipes	
Nu	Nusselt number, $(Nu = hD/k)$	dimensionless
Pr	Prandtl number, $(Pr = \mu c_p/k)$	dimensionless
Q	Heat transfer rate	W
R	Thermal resistance	$^{\circ}C.W^{-1}$
R_{time}	Working hours	hr
Re	Reynolds number, $(Re = \rho VD/\mu)$	dimensionless
S_L	Longitudinal pitch of the staggered arrangement	m
S_T	Transverse pitch of the staggered arrangement	m
T	Temperature	K
U	Overall heat transfer coefficient	$W.m^{-2}.K^{-1}$
Greek Symbols		
Δ	Difference	
ε	Effectiveness	dimensionless
η	Efficiency	dimensionless
ρ	Density	$kg.m^{-3}$

(*continued on next page*)

* Corresponding author. Heat Pipe and Thermal Management Research Group, Brunel University London, Uxbridge, UB8 3PH, UK.
E-mail address: hussam.jouhara@brunel.ac.uk (H. Jouhara).

https://doi.org/10.1016/j.energy.2025.134428
Received 23 September 2024; Received in revised form 24 November 2024; Accepted 6 January 2025
Available online 6 January 2025

(*continued*)

Symbols		Unit
σ	Surface tension	$N.m^{-1}$
μ	Dynamic viscosity	Pa.s
Subscripts		
c	Refers to condenser section	
ci	Internal surface of the condenser	
co	External surface of the condenser	
cond	Conduction	
e	Refers to evaporator section	
ei	Internal surface of the evaporator	
eo	External surface of the evaporator	
exp	Experimental	
f	Fin	
h	Hot	
hp	Heat Pipe	
HPHE	Heat Pipe Heat Exchanger	
l	Liquid	
L	Longitudinal	
max	Maximum	
o	Outer	
out	Outlet	
s	Wall surface	
sat	Saturation	
T	Transverse	
theo	Theoretical	
v	Vapour	

1. Introduction

In recent years, the process industries have been heavily scrutinised due to their excessive reliance on fossil fuels and generation of greenhouse gases being exhausted into the atmosphere. Process industries involving the processing of raw materials are responsible for approximately 23 % of emissions globally. Several global initiatives and strategies, in compliance with the Paris Agreement, aim to reduce greenhouse gas emissions by 50 % by 2030 compared to 1990 levels and to achieve net-zero carbon emissions by 2050. The roadmap presented by the European Union (EU) further enforces this by pledging to transform industry to a low carbon process by reducing emissions by up to 95 %, it aims for industries to place a heavy focus on circularity such as using recycled material. Current issues such as climate change and increasing fuel prices has developed an incentive for process industries to optimise the production plant but to also minimise costs whilst coping with the demand for raw materials. With historically high energy prices, the global necessity to reduce harmful emissions, governmental net zero policies and requirement for companies to demonstrate effective corporate and social responsibility, there is a large movement towards the installation of waste heat recovery technologies [1–3].

Energy intensive industries possess high excess heat potential in quantity and temperature which can reach up to 400 °C in metal and glass industries [4]. Miro, Brückner and Cabeza [5] studied the cumulative waste heat outputs of 33 countries and 6 subregions of different countries. The study highlighted the potential for Industrial Waste Heat (IWH) recovery across 6 main industrial categories. Fig. 1 presents and ranks the percentage of industry within these countries of which the 6 categories of industrial waste heat intensive industries apply. On average, 73.6 % of the industrials are classed as industrial waste heat intensive industries. This shows the large opportunity for waste heat recovery applications. In fact, waste heat recovery from industrial processes offers significant potential for low-temperature district heating systems, particularly with supply and return temperatures around 50/20 °C, which could contribute to decarbonisation of heating sector [6,7]. Furthermore, the grey bars represent industrial waste heat from industrial sectors that are not considered as IWH-intensive industries.

Several other technologies have been developed to capture and convert waste heat into a useable energy source [8–10]. One of the main technologies currently being proposed for the steel industry is the application of organic Rankine cycles (ORC). A study conducted by Walsh and Thornley [11] investigating the applicability of an ORC within the steel industry. The study identified the flue gas stream and as the source for low grade waste heat recovery. The technology solution proposed within the study successfully managed to recover low grade waste heat and reduce 10,000 t/CO2 per year but the economic analysis exceeded the industry standard by reporting a return on investment (ROI) of approximately 3–6 years. A similar study was conducted by Ramirez et al. [12] where an ORC was integrated within a steel mill, the flue gas was identified as the heat source. Unlike the study conducted by

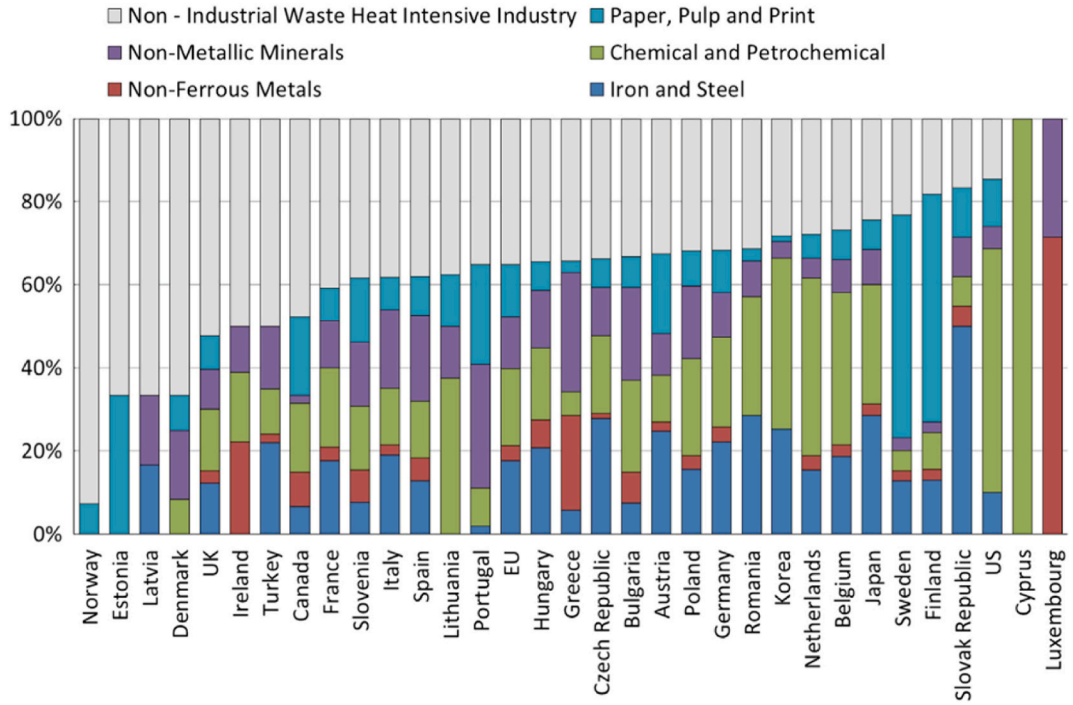

Fig. 1. Percentage of countries' Industry classed as 'Waste Heat Intensive' by 6 categories [5].

Walsh and Thornley [11], the ORC aims to produce superheated steam for an auxiliary heating system during winter and electricity for the remainder of the year. The unit also features an on/off function to harmonise inconsistent output with the production line, as a result an initial efficiency of 21.7 % was reported. The initial functionality and properties of the ORC are only reported but show a degree of success. A similar study was also conducted by Pili et al. [13] who investigated the feasibility of an ORC unit to recover waste heat from a rolling mill. The reported unit was investigated in combination with an energy storage unit with the aim to produce a steadier energy output. The study identified the exhaust gas as the heat source where several temperatures and flow rates were tested. Each case study investigated highlighted a positive trend in overall efficiency with the addition of energy storage, from an economic perspective, the addition of energy storage technologies within an ORC unit improved the overall ROI but estimates an overall ROI of 10 years. One of the key points raised within the study highlighted a key limitation of ORC technology: the lack of suitable heat sources but also the overestimation of theoretical and actual heat recovery. The focus on optimising the operational parameters of ORC cycles within the steel industry has been investigated by Jaafari and Rahimi [14]. The study combined an ORC with reverse osmosis system from wet cooling towers thus reducing the reliance on ground water sources. Both systems are presented as separate recovery loops, where the heat recovery is achieved via a heat exchanger placed within the flue stack, the subsequent generated electricity powered the reverse osmosis loop. The outcome of the study highlighted that the optimum configuration could reach 34.81 %. One of the key outcomes discussed in the study shows the trend of combined systems. For example, Zhang et al. [15], numerically investigated the performance of an ORC system to recover waste heat to be further applied in an urban heating application. The study presents an exergy analysis where various parameters and stages in production were investigated to gather the most optimum configuration for the proposed system. The study identified that the blast furnace and the processing of raw materials has the highest potential for waste heat recovery, followed by hot rolling. By applying an ORC cycle to such processes, the overall exergy efficiency increased by 1.71 %, and a total heating load equated to 229–251 MW which can satisfy the heating requirements of a 5.93 million m^2 area for four months. Similarly, Ja'fari et al. [16] investigated the viability of ORC within the steel and iron industries. Although the technology as potential for low grade waste heat recovery, the technology shows many developmental challenges to make the technology fully viable. For instance, several studies have highlighted inconsistencies in producing a constant supply of energy which may be counterproductive for reducing greenhouse gas emissions. Similarly, studies reflect the high investment required to implement ORC within a production line, several studies reflect that the typical ORC payback period is approximately 6 years. Other technologies for waste heat recovery within the steel industry include the installation of thermal energy storage. A study conducted by Schwarzmayr et al. [17], investigated the performance of a packed bed thermal energy storage within the steel industry. The proposed solution was tested and validated by lab scale unit which consisted of a cylindrical shell filled with an irregular and porous rock to facilitate a slow and constant release of energy to the heat transfer fluid. The role of the powder-gas heat transfer fluid is used to charge by absorbing heat from the exhaust of the furnace and discharge the packed bed thermal storage to the end user requirement. The packed bed was tested at various mass flow rates as reflected in the exhaust of a kiln, the outcome of the study highlighted a successful performance, but due to the two-phase nature of the heat transfer fluid several inconsistencies were reported which can affect the performance of the thermal energy storage. Slimani et al. [18], numerically investigated horizontal thermal energy storage systems for waste heat recovery within the steel industry. The proposed system uses the slag bricks as a thermal storage material, arranged in cylindrical passes to allow air to pass through. To simulate the storage cycles, alternate cycles were modelled, to ensure that the thermal cyclic conditions were close to realistic conditions as observed in the furnace. The outcome of the study showed that the preliminary results highlighted a discharge efficiency of 30 %, with an estimated greenhouse gas reduction of 88 kt. Although the preliminary seem promising, several optimisation processes are required to maximise the performance of horizontal thermal storage systems. Xue et al. [19] also investigated the role of molten salt based thermal energy storage solutions within the gas utilisation system within steel plants. The outcome of the study highlighted a successful operation whilst reporting a 4.93 % increase in overall system efficiency. Due to the complexity of the system, an estimated ROI of 4.9 years was reported. Moreover, multiple aspects should be considered for ranking of waste heat recovery technologies against each other such as: safety and risk, complexity of implementation, effectiveness, level of additional pressure drop, comparative scale of modification, and potential market opportunity [20]. Several studies highlight significant potential for development and future technologies, but each study signifies a fundamental issue which is the readiness of the technology and the overall payback of the technology. Further studies investigating the role of thermal storage within district heating report its functionality to provide a consistent thermal output from previously unstable heat sources [21].

In recent developments, several studies have investigated the applicability of thermoelectric generators (TEG) within the high temperature applications [22]. For example, Ochieng et al. [23] investigated the potential for TEG to be applied in low grade waste heat recovery. The initial analysis presented in the study shows a preliminary successful operation within the automotive industry to generate electricity from the exhaust of a car, but several challenges exist for the implementation within industrial waste heat recovery. The most notable being the low conversion efficiency. Many variables effecting the performance, such as: materials, positioning, geometry, operating conditions, and optimum configuration for process industries have also been reported. The study highlights that most commercially available materials for TEG's have a lower operating temperature and are unsuitable for high temperature applications such as metal processing plants. External conditions such as: inconsistent flow rates and temperature differences can also cause adverse effects to the efficiency. Ma et al. [24] also investigated the performance of TEGs for waste heat recovery, where several TEG configurations were tested alongside various flow rates and temperatures. The outcome of the study highlighted that approximately 300 °C was the maximum operation temperature with the highest efficiency but increasing the flow rate caused detriment to the performance. Similar results were reported by Lan et al. [25]where lower flow rates improved the overall efficiency of the TEG. Li et al. [26] developed a lab scale furnace to further characterise TEG performance at higher temperatures. A lab scale furnace was constructed to operate at 600 °C to mimic the thermal profile within a steel mill, the test operated incrementally noting performance at various set temperatures. A key finding from this study showed that without a cooling system for the circuitry, the system showed signs of failure at 240 °C. The study suggested further cooling loops should be added around the circuitry to prevent the solder from melting and to expand the applicability of TEG systems.

Furthermore, a study conducted by Ma et al. [27] suggests that heat exchangers can offer a path to efficient waste heat recovery, by estimating that approximately 60 % of mid-grade waste heat can be recovered. However, conventional heat exchangers encounter various challenges as waste heat recovery (WHR) solution such as fouling, thermal stress, harsh environment, limited weight and space availability, and cost, which limits their applicability and feasibility. Various studies have been conducted by Jouhara et al. [28], to investigate technologies aimed to improve the performance of process industries such as: burner technologies, waste heat boilers, heat exchangers, regenerators and recuperators. The outcome of the study suggested that one of the most efficient and scalable technologies suitable for industrial waste heat recovery was: heat pipe heat exchangers. The application of

heat pipes within the steel industry has been investigated by Jouhara et al. [29],where a novel flat heat pipe was developed to recover waste heat via radiation from the cooling section of hot wires. The lab scale unit (1m × 1m) was investigated in both laboratory and industrial conditions, to investigate the initial heat recovery potential. To determine the performance of the system, the system was tested at various inclination angles, temperatures and condenser flow rates. The initial results highlighted an overall recovery of 5 kW and shows significant potential to be expanded across the 70m production line. The system was further investigated by Almahmoud et al. [30],to maximise the performance of the novel flat heat pipe, a lab scale system (1m × 1m) was developed and tested in various configurations such as coatings and conditions including laboratory and industrial installations. The outcome of the study suggested that by coating the surface of the heat pipe in black thermal paint and including a back panel significantly increased the heat recovery by 570 % an unpainted system without a back panel. The lab scale unit was reported to recover 8.5 kW. Ma et al. [27] investigated the development of a lab scale heat pipe heat exchanger (HPHE), to determine the optimum conditions for applicability. The system was developed under laboratory conditions where the hot exhaust flow was represented via air being heated, similarly, the condenser stream was a freshwater pump. Interestingly, to mimic the pollutants of the exhaust flow, calcium and magnesium ions were deposited onto the heat pipes do mimic a fouling regime similar to an industrial unit and the subsequent effect of a cleaning system. The outcome of the study highlighted an improved heat transfer rate with an increase in condenser flow rate from 0.102 kW to 0.259 kW. Similarly, by including an online cleaning device further improved the heat transfer performance. To determine the most optimum waste heat recovery potentials in the steel industry, Llera et al. [31] further investigated the application of a HPHE to determine the recovery of steam within the steel industry. The outcome of the study highlighted that up to 65 % of the required steam was generated and can reduce costs by 29 % which would have occurred if a steam boiler was used. Similar trends were highlighted by Egilegor et al. [32], who reported the potential energy savings in the ceramic, steel and aluminium industry. One of the most notable observations made within the study highlights that excess energy from the flue gas accounts for approximately 20 % of energy input within the furnace, similarly approximately 12 % is recoverable by waste heat recovery solutions.

The main objective of this paper is to investigate a full-scale gravity-assisted Heat Pipe based Heat Exchanger (HPHE) as a WHR solution from challenging streams developed through the ETEKINA research project, which aims to improve the energy efficiency within energy-intensive industries, with a particular focus on the downstream process of the rolling mills in steel industry. As HPHEs are bespoke designs for each application, this HPHE was developed to recover heat from a challenging waste heat source and transfer it to two separate heat sinks: air and water. The exhaust stream was a challenging heat source stream due to the large sudden temperature and flow rate fluctuations causing mechanical and thermal stress ultimately making conventional heat exchangers economically unviable. Moreover, the HPHE was designed to offer the end-user the flexibility to bypass the water heat sink section and recovering heat to the combustion air solely. To enhance the energy efficiency of the process plant, the HPHE was designed to achieve waste heat recovery efficiency of more than 40 %. Thermal and economic performance of the HPHE is evaluated in this paper based on data collected from its operation in industrial environment. In addition, a theoretical modelling tool developed to predict the thermal performance of the HPHE, has been validated through the experimental results. The outcomes of this study offers a comprehensive framework for a practical implementation, scalability, and replicability of future use case scenarios.

2. Methodology

2.1. HPHE design

This section describes the design of the 350 kW multi-sink HPHE installed at SIJ Metal Ravne in Slovenia. General principles for the operation of HPHEs and the mechanisms and theory of heat transfer can be found in Refs. [33–35]. This HPHE is described as multi-sink as there are two discrete sections with differing heat sink fluids for separate end uses from the same heat source. The first section is an exhaust-to-combustion air counterflow heat pipe heat exchanger, the second section is an exhaust gas to water crossflow heat pipe heat exchanger. Each section is split into evaporator and condenser sections, with the condenser sitting above the evaporator. The evaporator is where the heat source passes, and the condenser section is where the heat sink passes. Both evaporator sections, located in the lower section of the HPHE, extract heat from the exhaust flow. The heat sink for the condenser section in the first section is combustion air, which is heated to promote more efficient combustion in the furnace. The second section heat sink is water for space heating and sanitary water preparation of the adjacent office space. Furthermore, as not all the hot water was required during the summer, some was sold as energy exports for sanitation purposes. A general arrangement of the HPHE system can be seen in Fig. 2 showing the direction of stream flows, the inlet and outlets and the location of the bypass. The exhaust gas enters the HPHE system through the evaporator of the first section (HPHE inlet), as it leaves the first section (HPHE section 1 outlet) it can either enters the second section then passes it to the stack (HPHE outlet) or it can bypass the second section to operate the first section only.

Table 1 shows the main design parameters of the HPHE; determined from onsite measurements under steady-state conditions. The exhaust gases temperature of a heat treatment furnace was reduced from 360 °C to 150 °C, with a flow rate of 6150 kg h^{-1}, to generate 180 °C combustion air for the burners from a 30 °C inlet at a flow rate of 6590 kg h^{-1}. There was already a recuperator installed prior to the HPHE. The water section increased the temperature of hot water from 70 °C to 90 °C at 3000 kg h^{-1}. The company has the ability to bypass or use the exhaust-to-water second stage depending on the price of primary energy and accounting for the additional requirement for space heating in the colder months allowing for further process versatility.

The HPHE thermal design and, consequently, the outlet exhaust temperature (i.e the amount of heat recovery) are subject to performance, practical, and economic considerations.

- Performance and cost-trade off: recovering more waste heat and further lowering the exhaust temperature enhances the HPHE effectiveness and significantly increases its heat transfer surface area, resulting in a higher pressure drop. This requires more powerful fans and auxiliary equipment leading to a higher manufacturing and installation costs, which impacts the economic viability of the system.
- Space and weight constraints: The available space and system weight need to be carefully considered during the design stage of the system to ensure that HPHE can be installed without facing any physical or structural barriers.
- Practical heat utilisation: The amount of heat recovery must be matched with a suitable heat sink or an industrial process capable of utilising the recovered heat. This maintains the system efficiency and cost-effectiveness without the need of install unnecessary auxiliary equipment.

The 558 smooth thermosyphons in the first counterflow section were 2018 mm long with an outer diameter of 28 mm. The evaporation and condenser sections were 1167 mm and 800 mm, respectively. The working fluids were Dowtherm A and distilled water in the exhaust-to-combustion air section, and distilled water in the exhaust-to-water

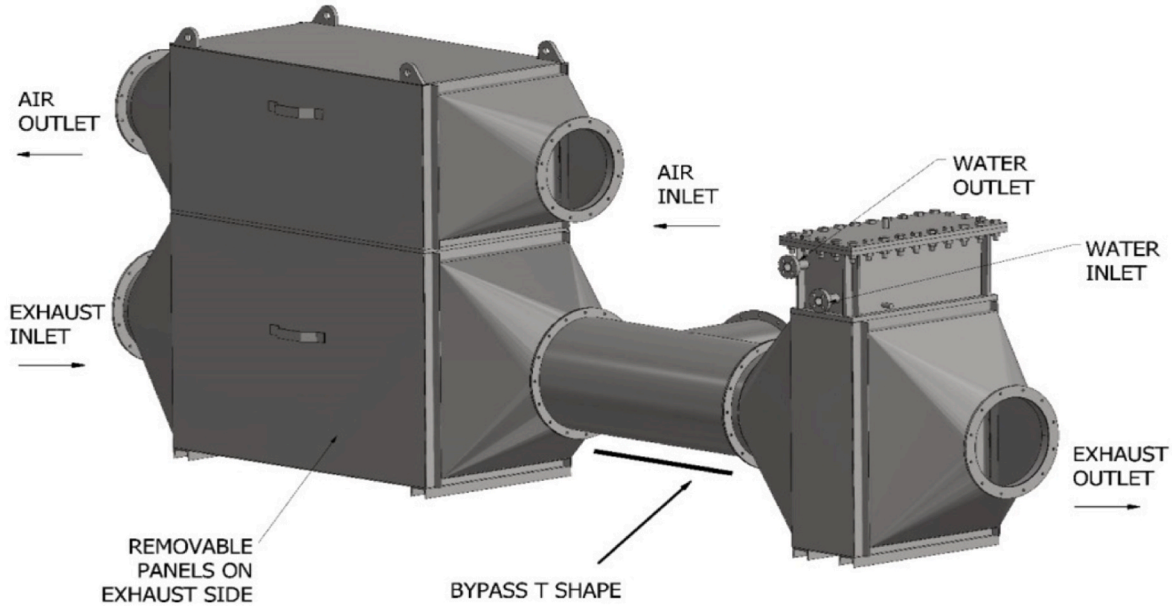

Fig. 2. General arrangement drawing of a the HPHE system.

Table 1
The main design parameters.

Parameter	Units
Exhaust inlet temperature	360 °C
Exhaust outlet temperature (to the ambient)	178.5 °C
Exhaust mass flow rate	6150 kg h^{-1}
Combustion air inlet temperature	30 °C
Combustion air outlet temperature	180 °C
Combustion air mass flow rate	6590 kg h^{-1}
Water inlet temperature	70 °C
Water outlet temperature	90 °C
Water mass flow rate	3000 kg h^{-1}
Thermal power recovered	349,989 W

section. The 126 smooth thermosyphons in the second crossflow section were 1500 mm long with an outer diameter of 28 mm, the evaporation and condenser sections were 1175 mm and 280 mm, respectively. All the thermosyphons are installed in a staggered arrangement. Splitting the HPHE into two sections using two different working fluids allows for a much higher temperature input as the maximum working temperature of the Dowtherm A thermosyphon bundle is higher than that of the water thermosyphon bundle, which were downstream and therefore experience cooler exhaust temperatures.

Figs. 3 and 4 show the arrangement, working fluid, direction of exhaust flow as well as the location of the thermocouples used for control purposes.

2.2. Implementation

The waste heat source was a steel billet preheating and heat treatment furnace (Allino). The waste heat contained in the exhaust gases has been harnessed to preheat the combustion air for the same furnace and provide hot water for the facility. An existing recuperator was already installed in the furnace exhaust stack, therefore, the source was already lowered in temperature prior to the installation of the HPHE.

Fig. 5 shows the physical installation of the multi-sink HPHE with

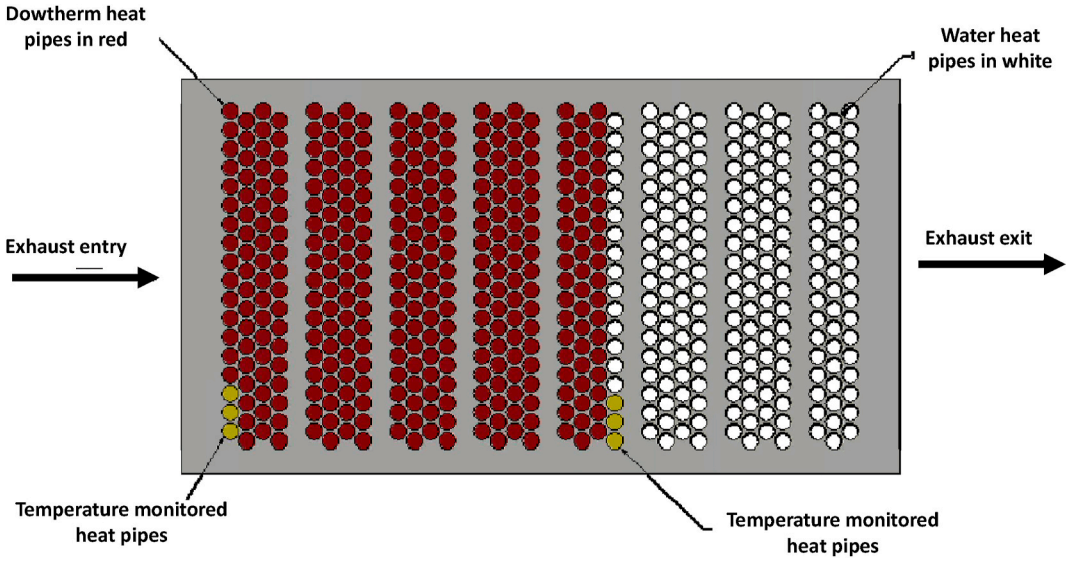

Fig. 3. Separation plate diagram showing the thermosyphon arrangement in the first combustion air section.

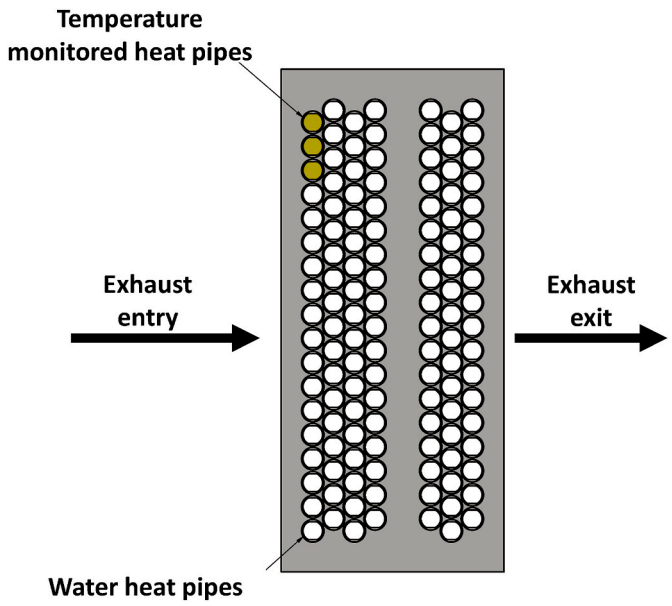

Fig. 4. Separation plate diagram showing the thermosyphon arrangement in the second water section.

both the combustion air and water sections. Each section was clad to minimise heat losses to the environment and increase thermal efficiency as HPHEs are more effective with a larger temperature difference between streams.

Fig. 6 shows a Piping and Instrumentation Diagram (P&ID) highlighting the main components of the waste heat recovery system. Bypasses were installed to either run the combustion air HPHE in isolation or in series with the water HPHE. In case of maintenance or fault, the entire system could be bypassed to return to previous operating conditions without waste heat recovery, where the exhaust gases are directed straight to the flue stack. The temperature of exhaust gases from the furnace fluctuates very quickly depending on the operation mode of the furnace. In order to ensure a steady operation of the HPHE heat recovery system, a temperature-controlled damper was installed, which allows dilution air to be added to exhaust source stream before entering the combustion air section. This was carried out to protect the HPHE from excessively high temperatures and to prevent unnecessary thermal expansion and contraction.

Fig. 7 (A) shows the control monitoring interface for the system installation and measurement locations. Fig. 7 (B) illustrates the sensors readings for the furnace chamber conditions and the waste heat recovery systems (ETEKINA HPHE and recuperator).

2.3. Theoretical modelling

2.3.1. Heat pipe modelling

Theoretical modelling of a HPHE is essential to predict and simulate its thermal performance represented by heat transfer rate and effectiveness at various operating conditions. Moreover, it allows optimising the design by fine-tuning dimensions and material selection to maximise the performance and reduce manufacturing cost.

The principle of a heat pipe allows the transfer of heat from hot exhaust stream to a cold heat sink stream by utilising the two-phase cycle within each heat pipe. When a heat source is in contact with the heat pipe wall, heat is transferred via forced convection. Subsequently the thermal conduction between the outer and inner pipe wall causes a boiling phenomenon within the working fluid inside the heat pipe. As a result, vapour is produced and due to a small difference in pressure between the evaporator and the condenser, the vapour rises to the condenser section. Once the saturated vapour reaches the condenser section it condenses and releases energy to the outer walls of the heat pipe via conduction and is subsequently transferred to the cold stream at the condenser side via forced convection. Finally, the condensate flows back to the evaporator by action of gravity in gravity-assisted heat pipes which are known as thermosyphons. Typically, the heat transfer process can be expressed as thermal resistances using electrical resistance analogy as shown in Fig. 8, similar to the representation of electrical resistances.

The total thermal resistance of a single heat pipe R_T can be shown as:

$$R_T = R_{eo} + R_{cond\_e} + R_{ei} + R_{ci} + R_{cond\_c} + R_{co} \quad (1)$$

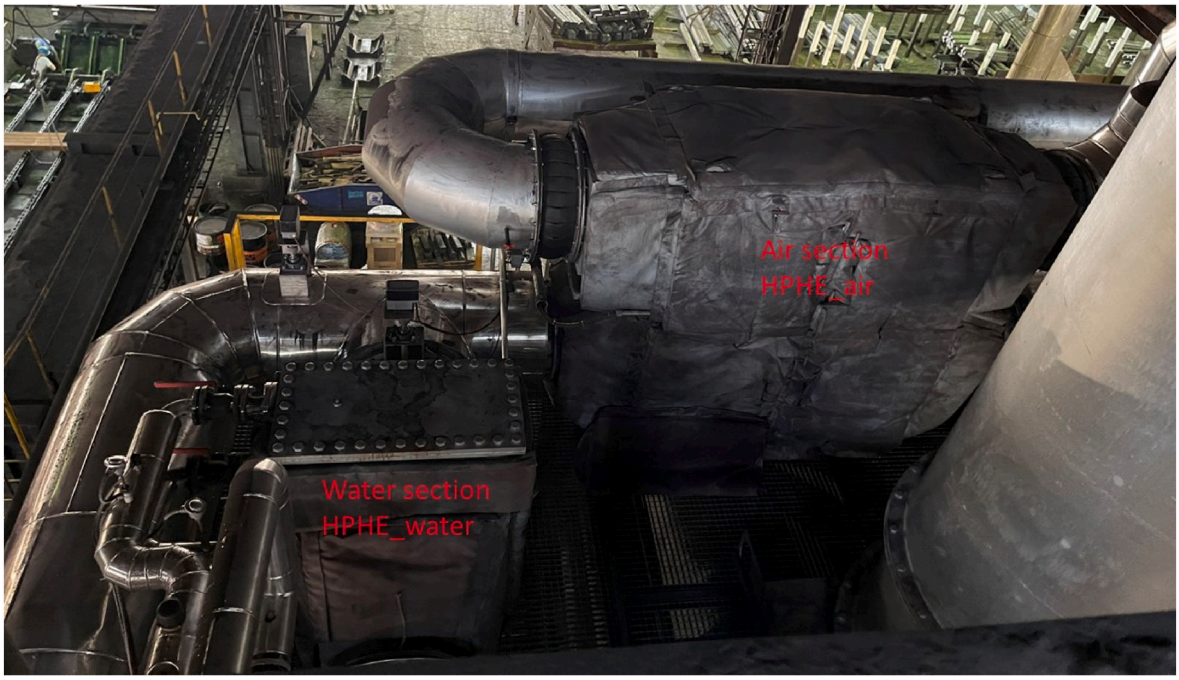

Fig. 5. Photo of the installation-two clad HPHE sections.

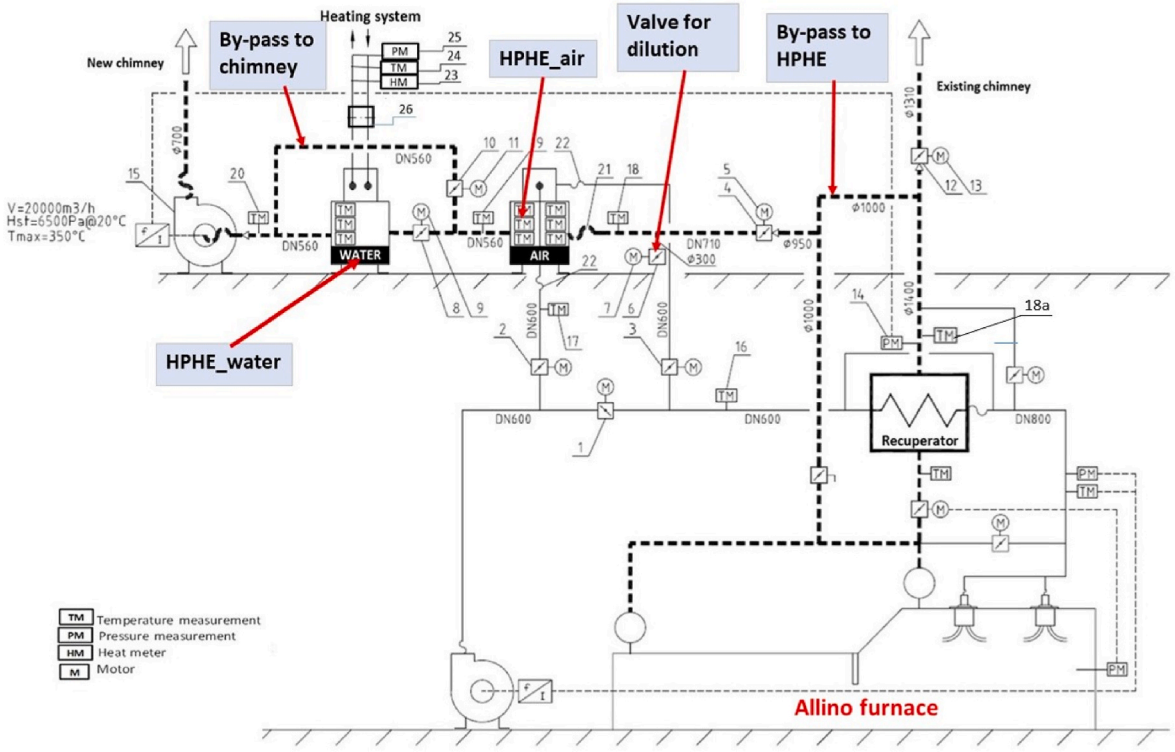

Fig. 6. P&ID of the installation.

where the resistances can be defined as:

R_{eo}: Force convective thermal resistance at the evaporator section ($K{\cdot}W^{-1}$)

R_{cond_e}: Conduction thermal resistance of the evaporator wall ($K{\cdot}W^{-1}$)

R_{ei}: Thermal resistance of boiling heat transfer ($K{\cdot}W^{-1}$)

R_{ci}: Thermal resistance of condensation heat transfer ($K{\cdot}W^{-1}$)

R_{cond_c}: Conduction thermal resistance through the wall of the condenser section ($K{\cdot}W^{-1}$).

R_{co}: Forced convection thermal resistance at the condenser side ($K{\cdot}W^{-1}$).

The boiling and condensation resistances: R_{ei} R_{ci} respectively are obtained from the relation between the thermal resistance and heat transfer coefficient as shown in Equation (2) and Equation (3):

$$R_{ei} = \frac{1}{h_{ei}A_{ei}} \tag{2}$$

$$R_{ci} = \frac{1}{h_{ci}A_{ci}} \tag{3}$$

where:

R_{ei} and R_{ci} represent the thermal resistance ($K.W^{-1}$), h the heat transfer coefficient ($W.m^{-2}.K^{-1}$) and A_{ei} and A_{ci} reflect the surface area of the respective evaporator and condenser section.

To determine the heat transfer coefficient for boiling, a correlation developed by Rohsenow [36] has been recommended for a wide range of applications:

$$h_{boiling} = \mu_l.h_{fg}\left[\frac{g.(\rho_l-\rho_v)}{\sigma}\right]^{\frac{1}{2}}.\left[\frac{C_p}{(C_{sf}.h_{fg}.Pr_l^n)}\right]^3.(T_{ei}-T_{sat})^2 \tag{4}$$

Where: μ_l is the liquid dynamic viscosity (Pa.s), h_{fg} is the latent heat of vaporisation ($J.kg^{-1}$), g is the gravitational acceleration ($m.s^{-2}$), both: ρ_l and ρ_v highlight liquid and vapour densities ($kg.m^{-3}$), σ is the working fluid surface tension ($N.m^{-1}$), C_p is the specific heat capacity ($J.kg^{-1}.K^{-1}$), C_{sf} is a constant which is dependent on the surface-fluid combination for this specific heat pipe shell material, working fluid combination which is 0.0132. Pr is the liquid Prandtl number which can also be expressed as: $Pr = \mu_l C_{p,l}/k_l$. Where k_l is the thermal conductivity of the liquid ($W.m^{-1}.K^{-1}$). Both T_{ei} and T_{sat} represent the temperature of the evaporator inner wall and saturation temperatures (°C) respectively.

The heat transfer coefficient for condensation can be defined using the Nusselt correlation [37–39] as shown in Equation (5).

$$h_{condensation} = 0.943\left[\frac{\rho_l(\rho_l-\rho_v)gh_{fg}k_l^3}{L_c\mu_l(T_{sat}-T_{ci})}\right]^{\frac{1}{4}} \tag{5}$$

Where: ρ_l and ρ_v reflect the liquid and vapour densities ($kg.m^{-3}$), h_{fg} is the latent heat of vaporisation ($J.kg^{-1}$), g is the gravitational acceleration ($m.s^{-2}$), k_l is the thermal conductivity of the liquid ($W.m^{-1}.K^{-1}$), μ_l is the liquid dynamic viscosity (Pa.s), L_c is the length of the condenser section (m), T_{ci} is the temperature of the condenser wall (°C). The definition of the radial conduction resistances of the heat pipe wall is shown in Equation (6) and Equation (7).

$$R_{cond,e} = ln(D_o/D_i)/(2\pi Lk_e) \tag{6}$$

$$R_{cond,c} = ln(D_o/D_i)/(2\pi L_c k_c) \tag{7}$$

Where, D_o and D_i reflect the respective external and internal diameters of the heat pipe (m). k_e and k_c denote the wall thermal conductivity ($W.m^{-1}.K^{-1}$) and L_e and L_c are the section lengths (m) at the respective evaporator and condenser sections.

The forced convection resistance at the evaporator R_{eo} and condenser R_{co} can be obtained by calculating the corresponding forced convection heat transfer coefficient and corresponding heat transfer area using Eq. (8). To determine the forced convection heat transfer coefficient of each pipe, the correlations by *Zukauskas* [40,41] can be used:

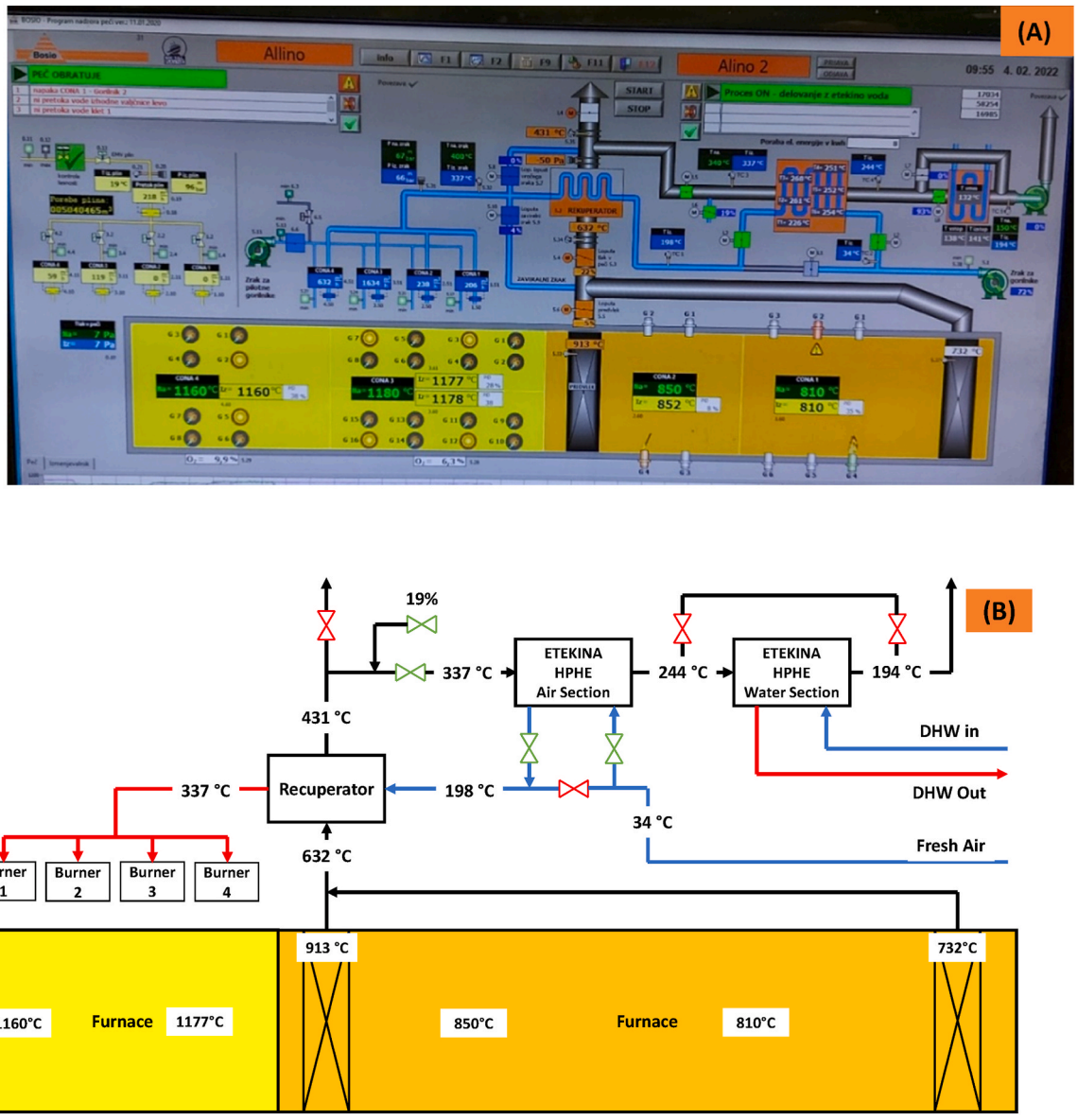

Fig. 7. Illustration of the control system for the heat recovery systems: (A) Control monitoring interface, (B) Simplified schematic of the control components layout and sensors readings.

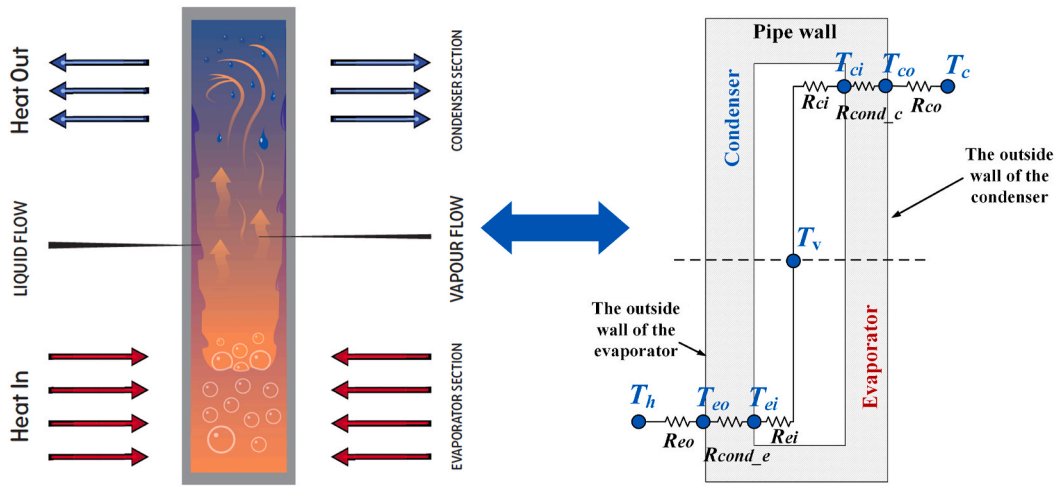

Fig. 8. Operation of a heat pipe and the corresponding thermal resistances.

$$Nu = \frac{h_{F.convection} D_o}{k} = 0.35(S_T/S_L)^{0.2} Re^{0.6}\, Pr^{0.36}(Pr/Pr_s)^{0.25} \quad for\ 1000 < Re < 2.10^5 \tag{8}$$

where Nu is the Nusselt number, $h_{F.convection}$ is the forced convection heat transfer coefficient ($W.m^{-2}.K^{-1}$), D_o is the external diameter of the heat pipe (m), k is the thermal conductivity of the fluid ($W.m^{-1}.K^{-1}$), χ_t^* is a ratio of transverse pitch to pipe diameter, χ_l^* is a ratio of longitudinal pitch to tube diameter, P_{fin} is the fin pitch, H_f is the fins height. Re is the Reynolds number, Pr and Pr_s are the Prandtl number of the flow and the Prandtl number at the surface temperature, respectively. S_T and S_L are the transverse pitch and longitudinal pitch of the staggered heat exchanger (m).

By adopting the electrical resistance analogy approach, a simplified HPHE can be modelled as shown in Fig. 9.

Given the resistance analogy, we can assume the heat pipes to be connected in parallel, where we can define the total thermal resistance (R_{HPHE}) as:

$$\frac{1}{R_{HPHE}} = \frac{1}{R_{hp,1}} + \frac{1}{R_{hp,2}} + \ldots \frac{1}{R_{hp,n-1}} + \frac{1}{R_{hp,n}} \tag{9}$$

where n denotes the number of heat pipes connected in parallel, and R represents the thermal resistance (°C/W). If we assume that each heat pipe has a similar thermal resistance, Equation (9) can be rewritten as:

$$R_{HPHE} = \frac{R_{hp}}{n} \tag{10}$$

By calculating the total thermal resistance of a heat pipe, the heat recovery can be determined by the following equation:

$$Q = \frac{\Delta T_{LM}}{R_{HPHE}} \tag{11}$$

Where: ΔT_{LM} represents the logarithmic mean temperature difference of the inlet and outlet of the exhaust streams and both condenser sections for counter current flows:

$$\Delta T_{LM} = \left(\frac{(\Delta T_1 - \Delta T_2)}{\ln\left(\frac{\Delta T_1}{\Delta T_2}\right)} \right) \tag{12}$$

$$\Delta T_1 = T_{hot,i} - T_{cold,o}$$

$$\Delta T_2 = T_{hot,o} - T_{cold,i}$$

By applying Equation (10), the heat recovery of the HPHE can expressed as:

$$Q_{HPHE} = UA\Delta T_{LM} \tag{13}$$

where UA is the HPHE overall conductance (W/°C).

2.3.2. Mean efficiency of heat recovery

The efficiency of instantaneous recovery in the primary side can be calculated by the following equation:

$$E = \frac{\dot{m}_{evap} \cdot Cp \cdot (T_{in} - T_{out})}{\dot{m}_{evap} Cp \cdot (T_{in} - T_{amb})} \tag{14}$$

Where T_{amb} represents the ambient temperature. An ambient temperature of 25 °C has been assumed.

2.3.3. Heat transfer rate

Heat transfer rate through the HPHE can be calculated from:

$$Q = \dot{m}_{exhaust} C_{P,exhaust} \left(T_{exhaust,in} - T_{exhaust,out}\right) \tag{15}$$

The useful energy recovered can be calculated for HPHE first and second section from:

$$Q = \dot{m}_{air} C_{P,air} \left(T_{air,in} - T_{air,out}\right) \tag{16}$$

$$Q = \dot{m}_{water} C_{P,water} \left(T_{water,in} - T_{water,out}\right) \tag{17}$$

3. Results

3.1. Temperature profiles, heat recovery rate and thermal efficiency

Although the waste heat recovery system is now in continuous operation, the analysis of the operation is based on the data provided for the period between November 2021 and March 2022. Since this period, there have been a few breaks in production due to maintenance activities or planned shutdowns. A sample of the data for the duration from 10th to January 17, 2022 is presented, and for steady-state operation, data from the 10th to January 16, 2022 has been selected.

Fig. 10 presents a graph showing the temperature profile of the exhaust gases stream in different areas of the system; prior to (Exhaust_source) and after (Exhaust_mix, HPHE inlet) the existing recuperator with dilution. It can be seen that the temperature of exhaust gases from the furnace fluctuates very quickly depending on the operation mode of the furnace. The temperature of the exhaust gases between the combustion air and water section (Exhaust HPHE section 1 outlet) and the exhaust temperature discharged to the ambient after the HPHE water section (Exhaust outlet to the ambient) are also shown.

The exhaust temperature from the furnace ranges from 292 °C to 516 °C. The dilution control allowed a stable exhaust inlet temperature around 340 °C at the HPHE combustion air section. The temperature of exhaust gases between the combustion air and water sections decreases to just below 250 °C. After the water section, the exhaust temperature is discharged around 180 °C to the chimney.

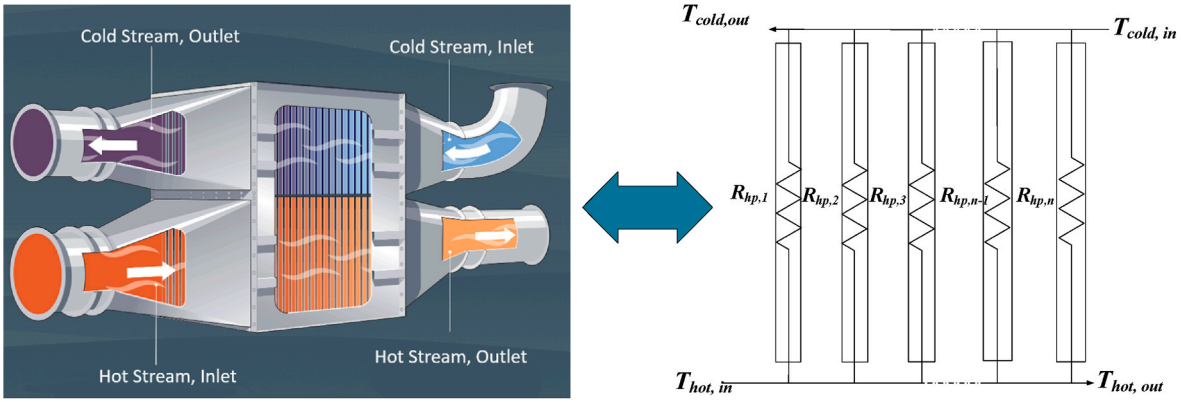

Fig. 9. Thermal resistance analogy used to develop a HPHE.

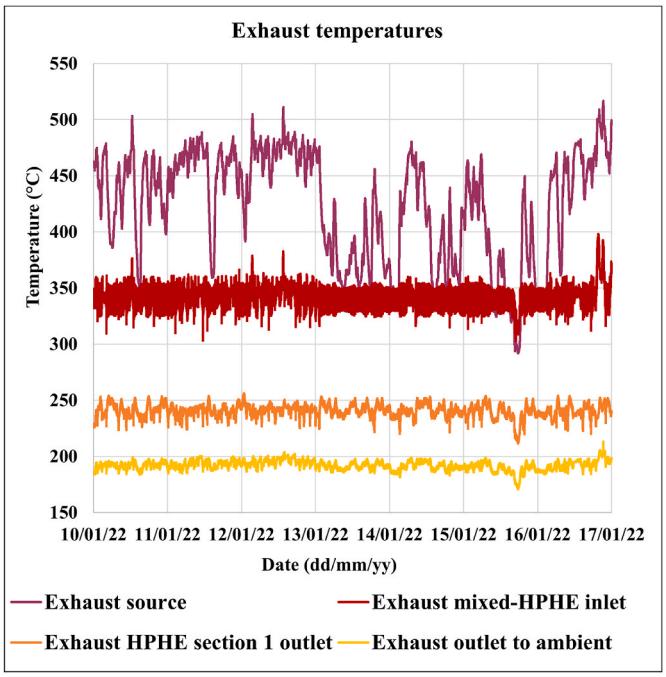

Fig. 10. Temperature profiles of exhaust gases for both sections of the HPHE.

Fig. 11 shows the operation temperatures of both streams exhaust and air of HPHE section 1. The combustion air temperature was raised from around 30 to 200 °C. It can be seen that the air outlet temperature was fluctuating due to variations in the exhaust inlet temperature.

Fig. 12 shows the inlet and outlet temperatures of the exhaust and water of the second HPHE section. The water temperature was raised from approximately 50 °C–70 °C. The fluctuations of the temperature profile are due to daytime and night-time operation.

In addition to temperature profiles, the mass flow rates of all the streams were monitored and controlled. This data is needed to determine the quantity of heat recovered. Fig. 13 shows the mass flow rates of

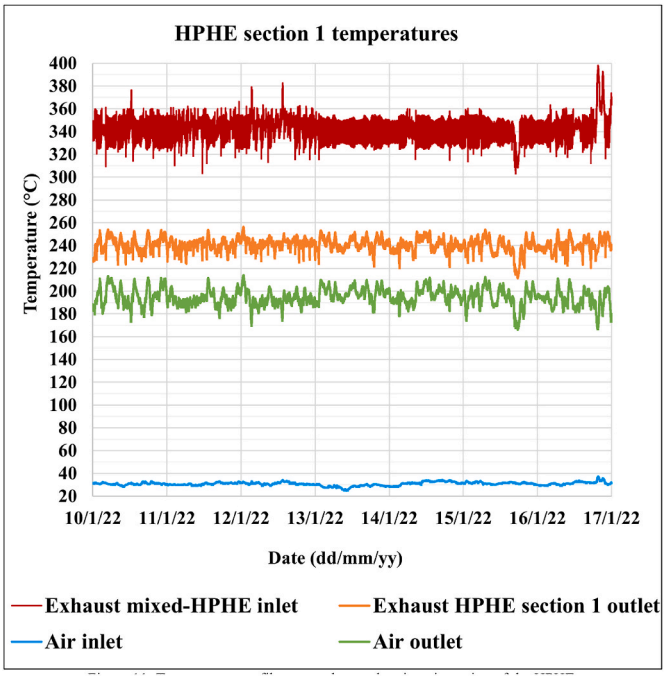

Fig. 11. Temperature profile across the combustion air section of the HPHE.

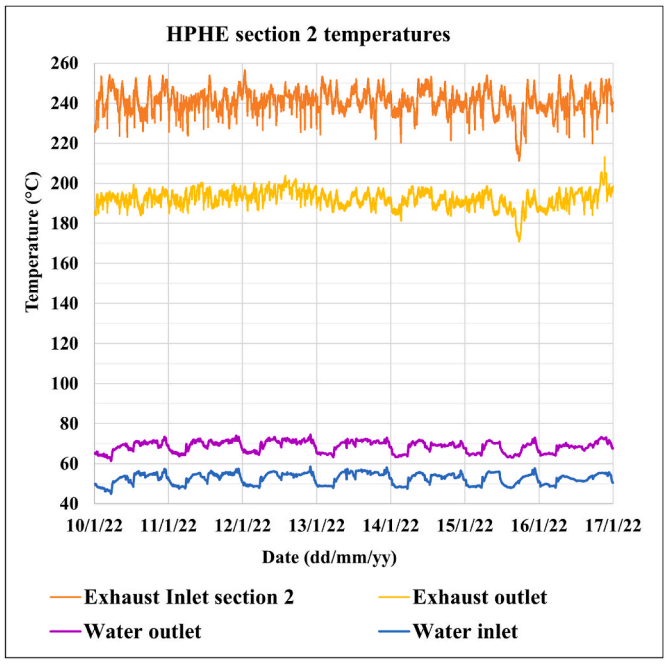

Fig. 12. Temperature profile across the water section of the HPHE.

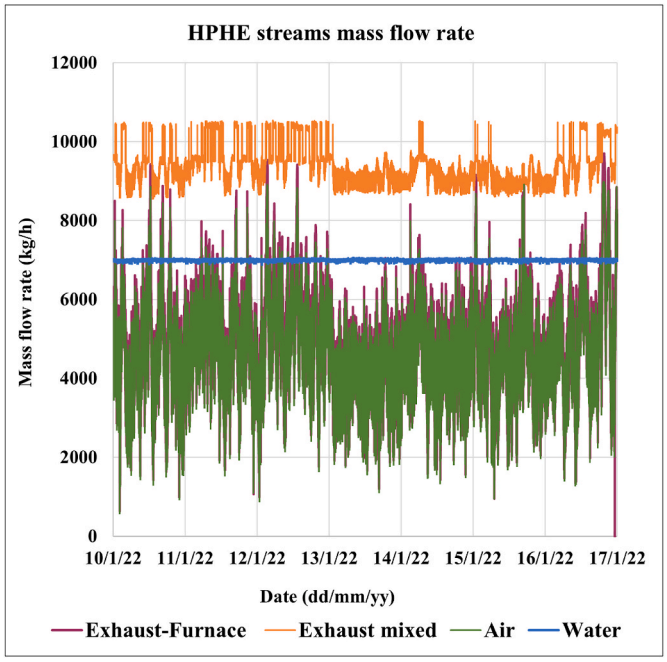

Fig. 13. Graph showing mass flow rate of exhaust, air and water.

the exhaust gases before dilution (Exhaust - Furnace/source), after dilution (Exhaust mixed), the combustion air (Air), and water. It can be noticed that the exhaust furnace and air flow rated were fluctuating based on the operation of the furnace.

Fig. 14 presents the heat recovery rate through the combustion air section of the HPHE. It can be seen that there was an evident difference between the heat absorbed from exhaust through HPHE and the heat transferred to the air side. In fact, this deviation is due to the location of the air outlet temperature probe, combined with the difference between the actual specific heat of the exhaust and the value applied for calculating the heat transfer rate. However, the heat transfer rate at the exhaust represents the actual heat duty recovered by the HPHE, while

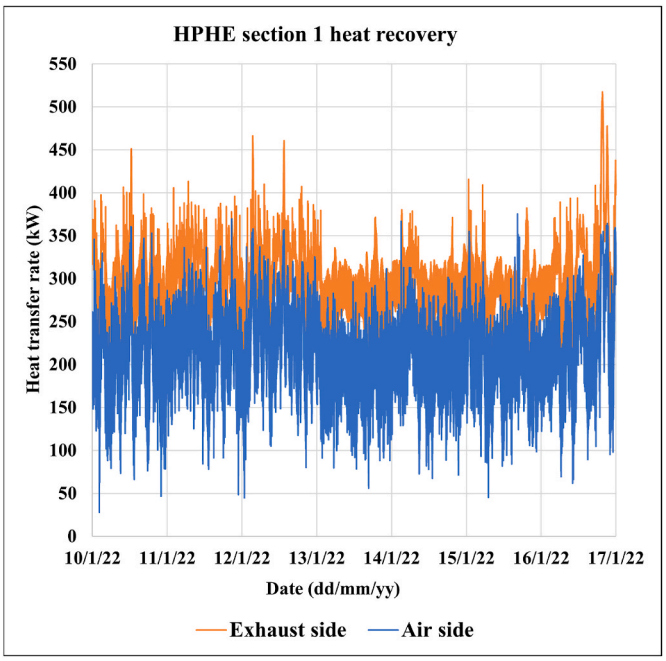

Fig. 14. HPHE section 1 (combustion air section) heat recovery rate.

the heat recovery at the air side represents the net useful heat recovery that contributes to energy saving following heat losses incurred through the ducts between the HPHE and the recuperator.The average heat recovery rate for the exhaust and combustion air section of the HPHE was 298 kW and 212 kW, respectively.

Fig. 15 shows the heat recovery rate through the water section of the HPHE. The average heat recovery rate at the water side for the second section of the HPHE was 130 kW. The deviation between the heat recovery calculated at the exhaust side and water side is due to the instantaneous changes in flue gas composition, flue gas dilution, which impacts specific heat capacity rate and flow rate measurements, and heat losses from the HPHE.

Useful heat recovery from each section, overall useful heat recovery of the HPHE system, and the overall heat efficiency of the HPHE are shown by Fig. 16. The HPHE exhibited an average heat efficiency of 47 % while the average useful heat recovery was around 342 kW.

3.2. *Theoretical modelling validation*

The theoretical model validation is presented in this paper along 4 h of experimental data. Fig. 17 presents the experimental and predicted temperatures of the exhaust and air streams through the first section of the HPHE. The predicted exhaust outlet temperature was close to the actual temperature. However, the fluctuation of the predicted temperature profile is primarily due to the fluctuating flow rate and inlet temperature. The thermal model was designed for steady state conditions and does not account for thermal lag caused by heat absorbed by the mass of the heat pipes. The actual data shows smoother fluctuations as the heat was absorbed by thermal mass of the heat pipes walls. The deviation of the prediction was 10 °C at the exhaust side, and 50 °C at the air side. As the model predicts the air outlet temperature directly after the HPHE unlike current position of the actual air temperature sensor.

Fig. 18 presents experimental and theoretical heat recovery through the first section of the HPHE. The heat recovered from the exhaust side was approximately 285 kW, while the useful heat recovery at the air side was 195 kW due to heat losses from the air duct and air flow leaks to the air outlet temperature sensor. The predicted heat recovery was about 253 kW, with an error of 11 % to the actual heat recovery from the exhaust.

Fig. 19 presents exhaust and water inlet and outlet temperatures through the second section of the HPHE. Predicted exhaust outlet temperature was very close to the actual exhaust outlet temperature. However, the actual exhaust outlet temperature exhibited smoother fluctuations compared to the predicted one. As detailed in previous sections, this is due to the model predicting an instantaneous response of the HPHE and neglects the thermal lag of heat absorbed by the heat pipe walls. Nonetheless, the predicted outlet temperature of water side was 2 °C higher than the experimental one. This difference is caused by the deviation between actual specific heat capacity of exhaust temperature, intensive variation of exhaust flow rate, heat losses from the HPHE which are neglected in the model.

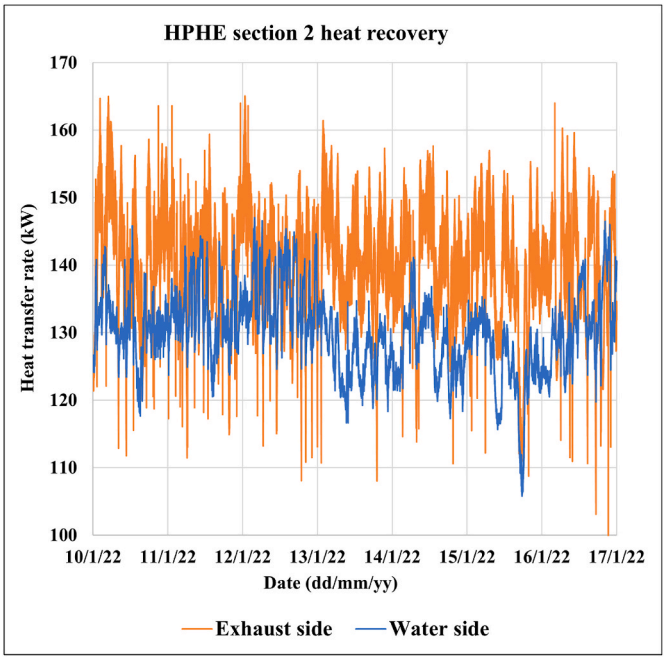

Fig. 15. Heat recovery rate for the second section of the HPHE (water section).

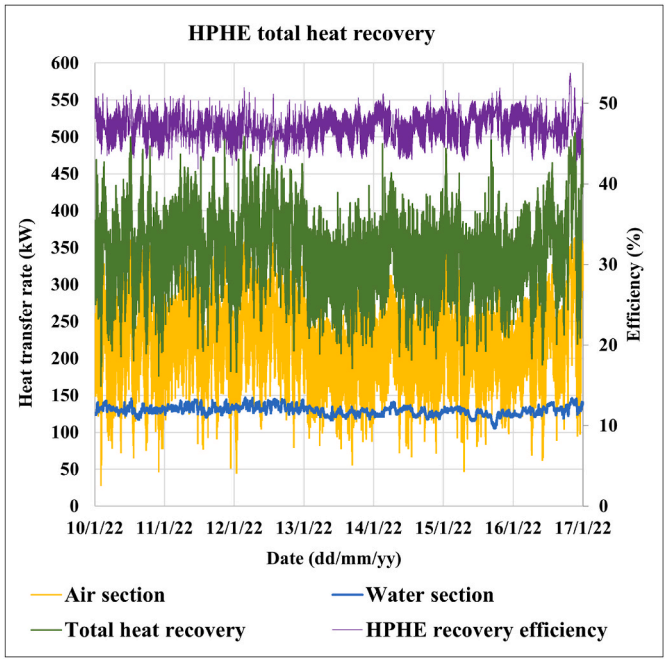

Fig. 16. Overall heat recovery and energy efficiency of the HPHE system.

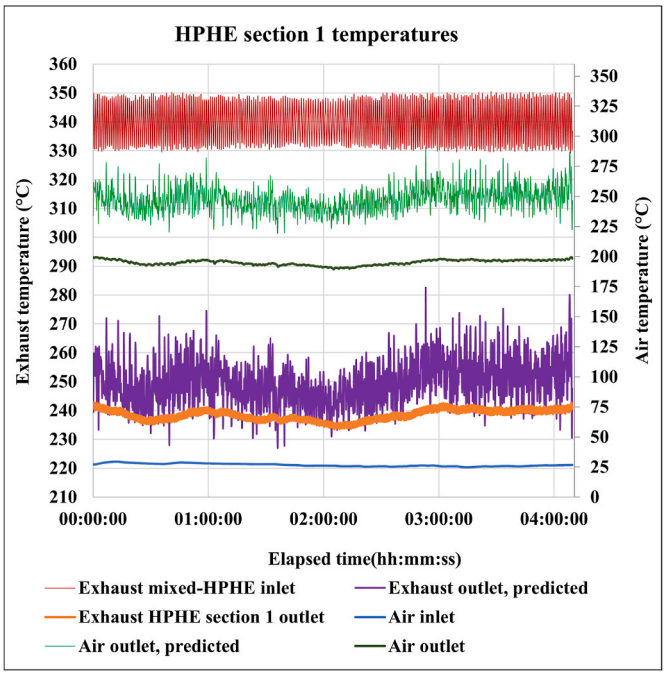

Fig. 17. Experimental and predicted temperatures of exhaust and air of HPHE section 1.

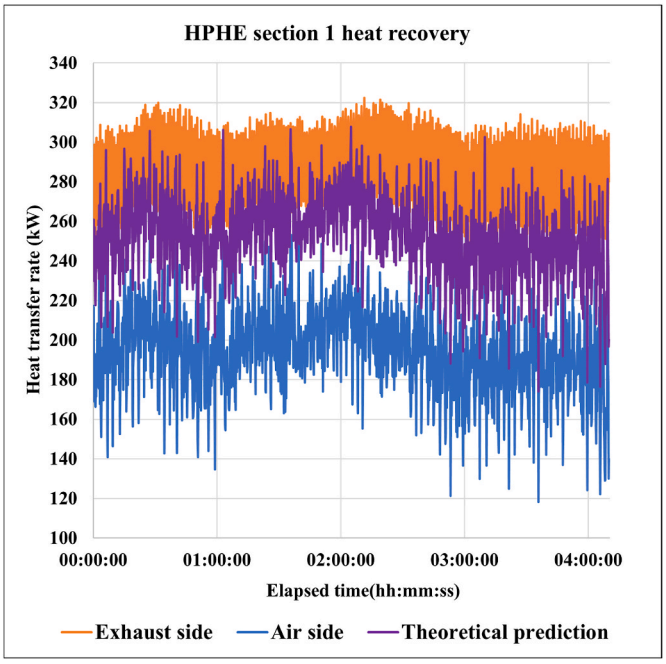

Fig. 18. Experimental and predicted heat recovery of HPHE section 1.

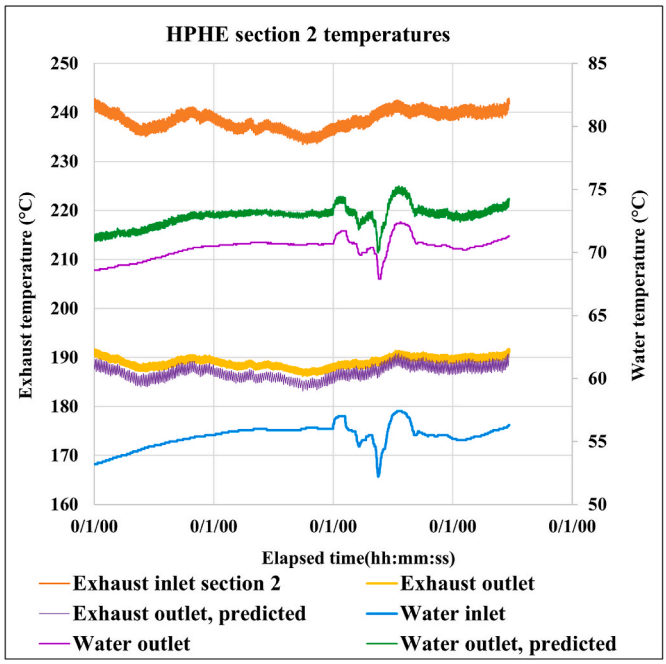

Fig. 19. Experimental and predicted temperatures of exhaust and air of HPHE section 2.

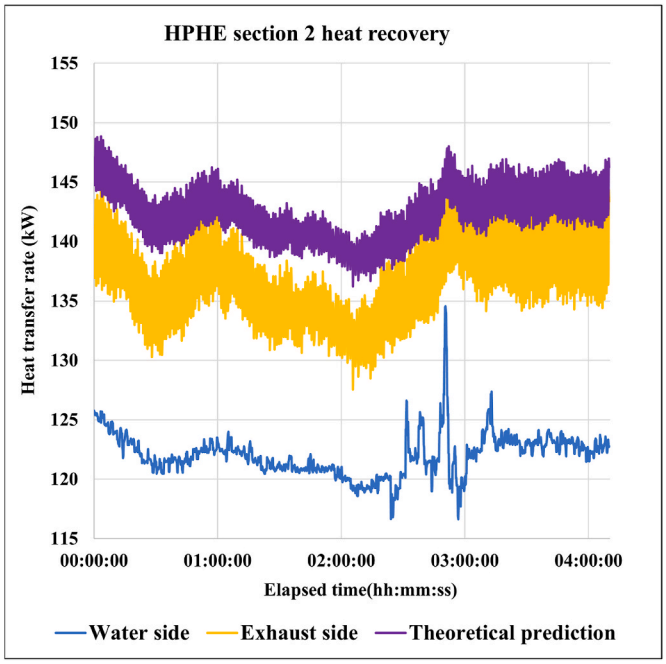

Fig. 20. Experimental and predicted heat recovery of HPHE section 2.

Fig. 20 presents the heat recovery through the second section of the HPHE. As it can be seen, the heat recovery absorbed from the exhaust side was around 137 kW, while the heat transferred to the water side was around 122 kW. The predicted heat recovery was approximately 142 kW.

Fig. 21 presents the experimental heat recovery through the HPHE of both section, and the predicted one. The predicted total heat recovery was very close to the actual one, but showing sharp fluctuations for the reasons explained previously.

Fig. 22 presents the predicted total heat recovery versus experimental total heat recovery data points. The theoretical model predicted most of the data points within an error of ±15 % which can be considered very good for a full-scale industrial application. The validated theoretical model can be used for scalability and reliability scenarios to predict the performance of HPHEs in different applications and identifying potential feasibilities. In addition, it validates the applicability of the two-phase heat transfer correlations for heat pipe modelling applications.

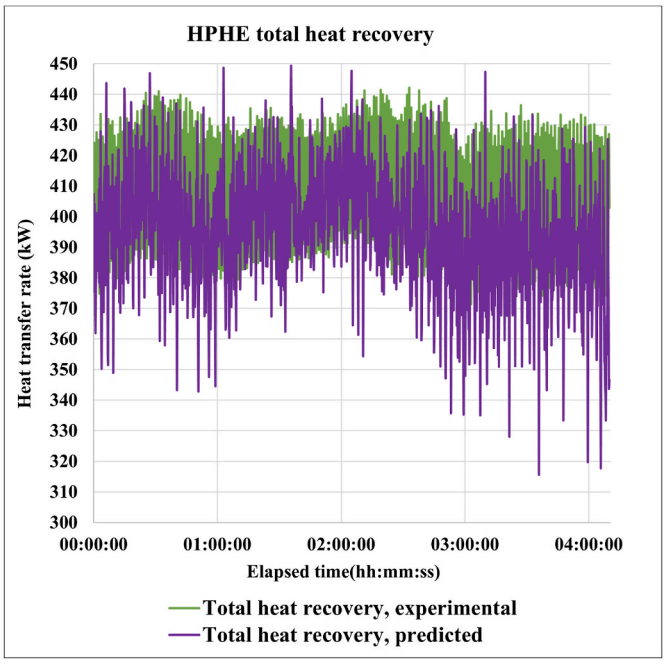

Fig. 21. Experimental and predicted HPHE total heat recovery of HPHE section.

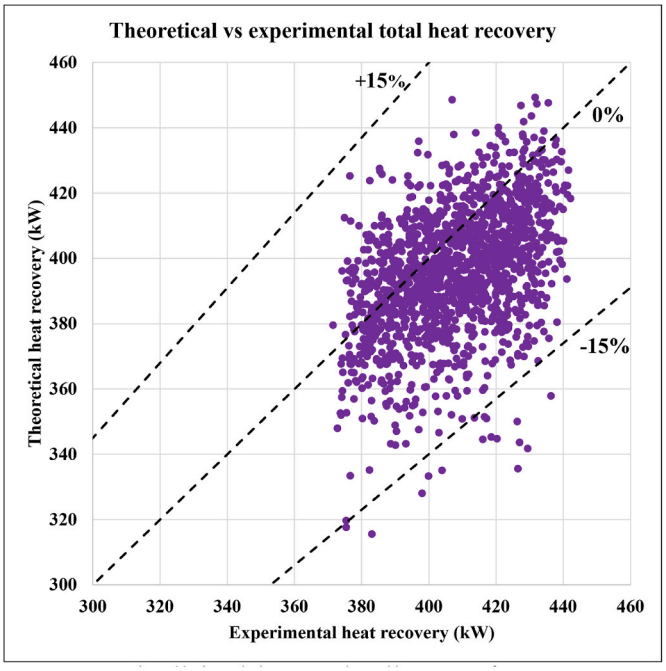

Fig. 22. Theoretical versus experimental heat recovery of HPHE.

3.3. Overall performance

The total heat recovered in the period between November 2021 and the end of March 2022, over 2804 operating hours, was 898 MWh. Of this, 534 MWh was recovered from the first exhaust-to-combustion air section and 364 MWh to the water section of the HPHE. The monthly amounts of recovered heat and the operation times of air and water sections of HPHE are shown in and Fig. 23.

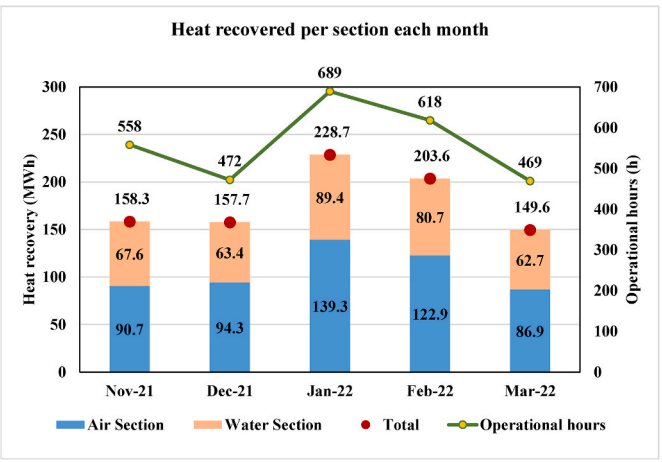

Fig. 23. Heat recovered according to section.

3.4. Economic analysis for measured period

This section presents the economic analysis for the results period presented between November 2021 and March 2022. The economic benefit for the company from the operation of the HPHE system was calculated from both the utilisation of excess heat, which resulted in reduced natural gas consumption in the furnace and also the reduction in CO_2 emissions. During the evaluation of the economic effects, the considered variables and value for each of the years 2021 and 2022 are shown in Table 2. Table 3 shows heat recovered, natural gas volume saved, savings, and CO_2 reduction by Month.

The total savings of natural gas over the period was 56,428 m^3, with a corresponding reduction in CO_2 emissions of 106 tCO_2. The total savings amounted to €65,092, of which €57,118 was attributed to recovered thermal energy and €7974 from avoided CO_2 emissions.

3.5. Economic analysis and ROI using yearly predictions

The measurement period results were used to extrapolate values for a year. This section presents yearly predictions and the projected return on investment for the HPHE system.

The prediction of the yearly heat recovery is calculated based on the average heat recovered per hour during the period of operation. The average recovered heat per hour value is calculated based upon the operation observed during the period shown by Fig. 24.

The average amount of weekly recovered heat is 57 MWh. 35 MWh (208 $kWh.h^{-1}$) average from the combustion air section and 22 MWh (131 $kWh.h^{-1}$) from the water section. The predicted annual energy savings is therefore 2430 MWh. 1677 MWh from the combustion air section of HPHE and 753 MWh from the water section. The savings in natural gas consumption equates to 177,177 $m^3\ yr^{-1}$, thereby reducing CO_2 emissions by 334 tCO_2 per year. The total economic impact is estimated at €198,050 per year. Of this, €173,013 can be attributed to

Table 2
Variables considered for the economic analysis.

Variable	Year	Value	Unit
Natural gas price	2021	31.2	€.MWh^{-1}
	2022	65.0	
CO_2 offset value	2021	75.0	€.tCO_2^{-1}
	2022	75.0	
Price from district heating system	2021	65.0	€.MWh^{-1}
	2022	85.0	
Calorific value of natural gas	2021	9.47	$kWh.m^{-3}$
	2022		
CO_2 emission factor	2021	0.199	$kg.MWh^{-1}$
	2022		

Table 3
Heat recovered with corresponding natural gas savings and CO_2 reduction.

Month	Section	Heat Recovered/MWh	Natural Gas Savings/m^3	Savings/€	CO_2 Reduction	
					t CO_2	€
Nov. 2021	Air	91	9582	3004	18	1354
	Water	68	–	4392	–	–
	Total	**158**	**9582**	**7396**	**18**	**1354**
Dec. 2021	Air	94	9965	3124	19	1408
	Water	63	–	4118	–	–
	Total	**158**	**9965**	**7242**	**19**	**1408**
Jan. 2022	Air	139	14,713	9053	28	2079
	Water	89	–	7603	–	–
	Total	**229**	**14,713**	**16,656**	**28**	**2079**
Feb. 2022	Air	123	12,984	7988	24	1835
	Water	81	–	6857	–	–
	Total	**204**	**12,984**	**14,845**	**24**	**1835**
Mar. 2022	Air	87	9184	5651	17	1298
	Water	63	–	5328	–	–
	Total	**150**	**9184**	**10,979**	**17**	**1298**
2021–2022	Air	534	56,428	28,820	106	7974
	Water	364	–	28,298	–	–
	Total	**898**	**56,428**	**57,118**	**106**	**7974**

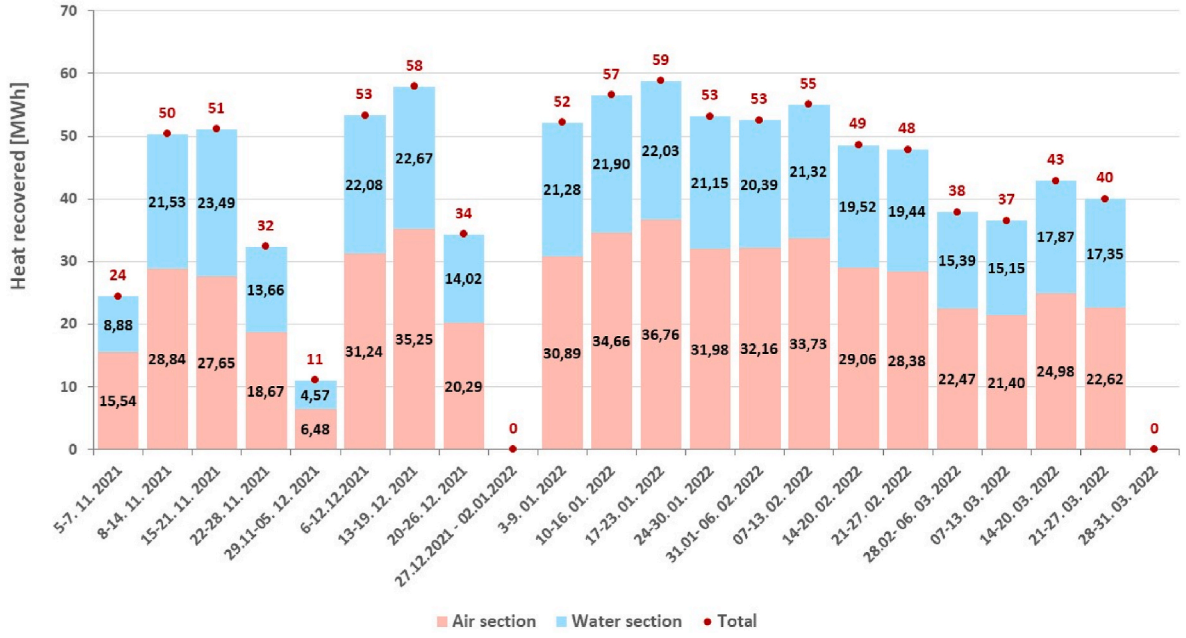

Fig. 24. Heat recovered per week in the period for both sections.

primary energy savings and €25,037 to the CO_2 emissions trading. These results are tabulated in Tables 4 and 5.

The savings attributed to the reduction of natural gas use are calculated based on the amount of heat recovered in the combustion air section of HPHE. The direct reduction of CO_2 emission is calculated on the basis of the saved amount of natural gas only. The heating system of the company is connected to the district heating system and therefore there is an additional indirect reduction of CO_2 emissions. Due to the reduction of demand for water for heating purposes from district heating, the CO_2 emissions were estimated at 279 tCO_2 per year, calculated based on the Slovenian average of CO_2 emissions by MWh of heat produced in district heating.

The total investment to install the system was €154,438 and therefore return of investment is estimated at 9.4 months.

Table 4
Predicted yearly energy recovered and savings.

	Operational time	Heat recovery rate		Energy price	Savings
	$h.yr^{-1}$	$kWh.h^{-1}$	$MWh.yr^{-1}$	$€.MWh^{-1}$	$€.yr^{-1}$
Combustion air section	8050	208	1677	65.0	109,010
Water section	5750	131	753	85.0	64,003
Total		339	2430		**173,013**

Table 5
Predicted yearly natural gas savings and CO_2 reduction.

	Natural gas reduction	CO_2 reduction			
	$Sm^3.yr^{-1}$	$t_{CO2}.MWh^{-1}$	$t_{CO2}.yr^{-1}$	$€.t_{CO2}^{-1}$	$€.yr^{-1}$
Combustion air section	177,177	0.199	334	75	**25,037**

4. Conclusion

A waste heat recovery system using a multi-sink HPHE has been successfully installed at a steelworks in Slovenia to preheat combustion air and heat water using the exhaust of a heating furnace. The design of the HPHE, the individual heat pipes, arrangement, separation plate and PID have been shown. Alongside an accurate theoretical model able to create a performance profile to indicate the operation of the unit. Given that the unit experienced ranges of fluctuation throughout operation, the HPHE thermal performance model was in good agreement with the experimental results. The experimental thermal recovery within the first section was 285 kW whereas the theoretical was 253 kW only highlighting an 11 % variation. The second section highlighted an experimental value of 122 kW, whereas the theoretical model was 142 kW, with an overall 16 % difference, and a 15 % variation across the whole system.

The validated theoretical prediction tool developed within the study acts as an initial development stage for the development of a full-scale replicability tool suitable for an industrial level. Due to the flexibility of heat pipe design and the ease of the tool presented within this study, the applicability of HPHE technology has become more accessible for challenging industries and exhaust compositions. The system has now shown a reliable track record of operation. The thermal results over five months of operation are presented. Results for this period have been extrapolated to present results for a yearly period. There has been an estimated natural gas consumption reduction of 177,177 Sm^3 per year. This reduction in natural gas consumption has reduced emissions of CO_2 by 334t per year. The net financial benefit for the company of natural gas reduction, CO_2 reduction and selling hot water equated to €173,013 per year meaning the system was paid back in less than 10 months. These improvements allow increased competitivity for the company as well as demonstrating a positive step of social and corporate responsibility.

CRediT authorship contribution statement

Hussam Jouhara: Writing – review & editing, Writing – original draft, Supervision, Resources, Investigation, Funding acquisition, Formal analysis, Conceptualization. **Bertrand Delpech:** Validation, Formal analysis, Data curation. **Sulaiman Almahmoud:** Visualization, Validation, Formal analysis, Data curation. **Amisha Chauhan:** Validation, Formal analysis, Data curation. **Fouad Al-Mansour:** Writing – original draft, Formal analysis, Data curation. **Matevz Pusnik:** Writing – original draft, Formal analysis, Data curation. **Alojz Buhvald:** Validation. **Kristijan Plesnik:** Validation.

Declaration of competing interest

The authors declare that they have no known competing financial interests or personal relationships that could have appeared to influence the work reported in this paper.

Acknowledgment

The presented work is part of HEAT PIPE TECHNOLOGY FOR THERMAL ENERGY RECOVERY IN INDUSTRIAL APPLICATIONS — ETEKINA project. The project has received funding from the European Union's Horizon 2020 research and innovation programme under grant agreement NO 768772.

"Heat pipe technology for thermal energy recovery in industrial applications" (
https://www.etekina.eu/, H2020-EE-2017-PPP- 768772)

Data availability

Data will be made available on request.

References

[1] Jouhara H. Waste heat recovery in process industries. first ed. Wiley; 2022.
[2] Jouhara H. Heat Pipes (Gravity Assisted and Capillary-Driven). In: Heat Exchanger Design Handbook. Begell House; 2019.
[3] Malinauskaite J, Jouhara H, Egilegor B, Al-Mansour F, Ahmad L, Pusnik M. Energy efficiency in the industrial sector in the EU, Slovenia, and Spain, vol. 208; 2020. https://doi.org/10.1016/j.energy.2020.118398.
[4] Moreno D, Nielsen S, Sorknæs P, Lund H, Thellufsen JZ, Mathiesen BV. Exploring the location and use of baseload district heating supply. What can current heat sources tell us about future opportunities? Energy 2024;288:129642. https://doi.org/10.1016/J.ENERGY.2023.129642.
[5] Miró L, Brückner S, Cabeza LF. Mapping and discussing Industrial Waste Heat (IWH) potentials for different countries, vol. 51; 2015. p. 847–55. https://doi.org/10.1016/j.rser.2015.06.035.
[6] Yuan M, Vad Mathiesen B, Schneider N, Xia J, Zheng W, Sorknæs P, et al. Renewable energy and waste heat recovery in district heating systems in China: A systematic review. Energy 2024;294:130788. https://doi.org/10.1016/J.ENERGY.2024.130788.
[7] Lund H, Werner S, Wiltshire R, Svendsen S, Thorsen JE, Hvelplund F, et al. 4th Generation District Heating (4GDH): integrating smart thermal grids into future sustainable energy systems. Energy 2014;68:1–11. https://doi.org/10.1016/J.ENERGY.2014.02.089.
[8] Jouhara H, Khordehgah N, Almahmoud S, Delpech B, Chauhan A, Tassou SASA. Waste heat recovery technologies and applications. Therm Sci Eng Prog 2018;6:268–89.
[9] Jaber H, Herez A, Lemenand T, Ramadan M, Khaled M. Experimental study on heat recovery from exhaust gas of chimneys using multi-tube tank: Effect of changing the head shape. International Journal of Thermofluids 2023;20:100518. https://doi.org/10.1016/J.IJFT.2023.100518.
[10] Orido GO, Ronoh EK, Ajwang PO, Gathitu BB. Performance assessment of hybrid recuperative heat exchanger for diesel engine generated exhaust gas. International Journal of Thermofluids 2023;19:100392. https://doi.org/10.1016/J.IJFT.2023.100392.
[11] Walsh C, Thornley P. Cost Effective Greenhouse Gas Reductions in the Steel Industry from an Organic Rankine Cycle. Chem Eng Trans 2011;25:905–10. https://doi.org/10.3303/CET1125151. SE-Research Articles.
[12] Ramirez M, Epelde M, de Arteche MG, Panizza A, Hammerschmid A, Baresi M, et al. Performance evaluation of an ORC unit integrated to a waste heat recovery system in a steel mill. Energy Proc 2017;129:535–42. https://doi.org/10.1016/j.egypro.2017.09.183.
[13] Pili R, García Martínez L, Wieland C, Spliethoff H. Techno-economic potential of waste heat recovery from German energy-intensive industry with Organic Rankine Cycle technology. Renew Sustain Energy Rev 2020;134:110324. https://doi.org/10.1016/j.rser.2020.110324.
[14] Jaafari R, Rahimi AB. Determination of optimum organic Rankine cycle parameters and configuration for utilizing waste heat in the steel industry as a driver of receive osmosis system. Energy Rep 2021;7:4146–71. https://doi.org/10.1016/j.egyr.2021.06.065.
[15] Zhang L, Na H, Yuan Y, Sun J, Yang Y, Qiu Z, et al. Integrated optimization for utilizing iron and steel industry's waste heat with urban heating based on exergy analysis. Energy Convers Manag 2023;295:117593. https://doi.org/10.1016/j.enconman.2023.117593.
[16] Ja'fari M, Khan MI, Al-Ghamdi SG, Jaworski AJ, Asfand F. Waste heat recovery in iron and steel industry using organic Rankine cycles. Chem Eng J 2023;477:146925. https://doi.org/10.1016/j.cej.2023.146925.
[17] Schwarzmayr P, Birkelbach F, Walter H, Javernik F, Schwaiger M, Hofmann R. Packed bed thermal energy storage for waste heat recovery in the iron and steel industry: A cold model study on powder hold-up and pressure drop. J Energy Storage 2024;75:109735. https://doi.org/10.1016/j.est.2023.109735.
[18] Slimani H, Filali Baba Y, Ait Ousaleh H, Elharrak A, El Hamdani F, Bouzekri H, et al. Horizontal thermal energy storage system for Moroccan steel and iron industry waste heat recovery: numerical and economic study. J Clean Prod 2023;393:136176. https://doi.org/10.1016/j.jclepro.2023.136176.
[19] Xue X, Liu X, Zhang A, Zhang L, Jin K, Zhou H. Performance and economic analysis of a molten salt furnace thermal energy storage and peaking system coupled with thermal power units for iron and steel gas waste heat recovery. Appl Energy 2024;363:123021. https://doi.org/10.1016/j.apenergy.2024.123021.
[20] Faqihi B, Ghaith F. A comprehensive review and evaluation of heat recovery methods from gas turbine exhaust systems. International Journal of Thermofluids 2023;18:100347. https://doi.org/10.1016/J.IJFT.2023.100347.
[21] Sihvonen V, Ollila I, Jaanto J, Grönman A, Honkapuro S, Riikonen J, et al. Role of power-to-heat and thermal energy storage in decarbonization of district heating. Energy 2024;305:132372. https://doi.org/10.1016/j.energy.2024.132372.
[22] Olabi AG, Al-Murisi M, Maghrabie HM, Yousef BAA, Sayed ET, Alami AH, et al. Potential applications of thermoelectric generators (TEGs) in various waste heat recovery systems. International Journal of Thermofluids 2022;16:100249. https://doi.org/10.1016/j.ijft.2022.100249.
[23] Ochieng AO, Megahed TF, Ookawara S, Hassan H. Comprehensive review in waste heat recovery in different thermal energy-consuming processes using thermoelectric generators for electrical power generation. Process Saf Environ Protect 2022;162:134–54. https://doi.org/10.1016/j.psep.2022.03.070.
[24] Ma X, Hu S, Hu W, Luo Y, Cheng H. Experimental investigation of waste heat recovery of thermoelectric generators with temperature gradient. Int J Heat Mass Tran 2022;185:122342. https://doi.org/10.1016/j.ijheatmasstransfer.2021.122342.

[25] Lan Y, Lu J, Wang S. An experimental study on the performance of TEGs using uniform flow distribution heat exchanger for low-grade thermal energy recovery. Energy 2024;292:130506. https://doi.org/10.1016/j.energy.2024.130506.
[26] Li X, Meng X, Miao Z, Liang B, Zou Q. Exploration and optimization on thermoelectric conversion of waste heat of blast furnace slag. Appl Therm Eng 2024;245:122889. https://doi.org/10.1016/j.applthermaleng.2024.122889.
[27] Ma H, Du N, Zhang Z, Lyu F, Deng N, Li C, et al. Assessment of the optimum operation conditions on a heat pipe heat exchanger for waste heat recovery in steel industry. Renew Sustain Energy Rev 2017;79:50–60. https://doi.org/10.1016/j.rser.2017.04.122.
[28] Jouhara H, Chauhan A, Nannou T, Almahmoud S, Delpech B, Wrobel LCC. Heat pipe based systems - advances and applications. Energy 2017;128:729–54. https://doi.org/10.1016/j.energy.2017.04.028.
[29] Jouhara H, Almahmoud S, Chauhan A, Delpech B, Bianchi G, Tassou SA, et al. Experimental and theoretical investigation of a flat heat pipe heat exchanger for waste heat recovery in the steel industry. Energy 2017;141:1928–39. https://doi.org/10.1016/j.energy.2017.10.142.
[30] Almahmoud S, Jouhara H. Experimental and Theoretical Investigation on a Radiative Flat Heat Pipe Heat Exchanger. Energy 2019. https://doi.org/10.1016/J.ENERGY.2019.03.027.
[31] Llera R, Vigil M, Díaz-Díaz S, Martínez Huerta GM. Prospective environmental and techno-economic assessment of steam production by means of heat pipes in the steel industry. Energy 2022;239:122334. https://doi.org/10.1016/j.energy.2021.122334.
[32] Egilegor B, Jouhara H, Zuazua J, Al-Mansour F, Plesnik K, Montorsi L, et al. ETEKINA: Analysis of the potential for waste heat recovery in three sectors: Aluminium low pressure die casting, steel sector and ceramic tiles manufacturing sector. International Journal of Thermofluids 2020;1–2:100002. https://doi.org/10.1016/J.IJFT.2019.100002.
[33] Faghri A. Heat pipe science and technology. second ed. Global Digital Press; 2016.
[34] Shabgard H, Allen MJ, Sharifi N, Benn SP, Faghri A, Bergman TL. Heat pipe heat exchangers and heat sinks: opportunities, challenges, applications, analysis, and state of the art. Int J Heat Mass Tran 2015;89:138–58. https://doi.org/10.1016/j.ijheatmasstransfer.2015.05.020.
[35] Ramos JAGSB. Experimental investigation and CFD modelling of a thermosyphon-equipped heat exchanger used in low-grade waste heat recovery. University of South Wales; 2016.
[36] Rohsenow WM, Hartnett JP. In: Rohsenow Warren M, Hartnett JP, editors. Handbook of heat transfer. Mcgraw-Hill; 1973.
[37] Nusselt W. The condensation of steam on cooled surfaces. Z Ver Dtsch Ing 1916;60:541–6.
[38] Incropera FP, DeWitt DP, Bergman TL, Lavine AS. Fundamentals of heat and mass transfer. Fundamentals of Heat and Mass Transfer 2007;997. https://doi.org/10.1016/j.applthermaleng.2011.03.022.
[39] Jouhara H, Reay D, McGlen R, Kew P, McDonough J. Chapter 4 - heat transfer and fluid flow theory. In: Jouhara H, Reay D, McGlen R, Kew P, McDonough J, editors. Heat pipes. seventh ed.). seventh ed. Butterworth-Heinemann; 2024. p. 127–207. https://doi.org/10.1016/B978-0-12-823464-8.00011-5.
[40] Kakac S, Shah RK, Aung W. Handbook of single-phase convective heat transfer. United States: John Wiley and Sons Inc; 1987.
[41] Žukauskas A. Heat transfer from tubes in crossflow. Adv Heat Tran 1972;8:93–160. https://doi.org/10.1016/S0065-2717(08)70038-8.